



An anomalous extra Z prime from intersecting branes with Drell–Yan and direct photons at the LHC

Roberta Armillis^a, Claudio Corianò^{a,b,*}, Marco Guzzi^a, Simone Morelli^a

^a *Dipartimento di Fisica, Università del Salento and INFN Sezione di Lecce, Via Arnesano, 73100 Lecce, Italy*

^b *Department of Physics and Institute of Plasma Physics, University of Crete, 71003 Heraklion, Greece*

Received 10 December 2008; received in revised form 3 January 2009; accepted 19 January 2009

Available online 27 January 2009

Abstract

We quantify the impact of gauge anomalies at the Large Hadron Collider by studying the invariant mass distributions in Drell–Yan and in double prompt photon, using an extension of the Standard Model characterized by an additional anomalous $U(1)$ derived from intersecting branes. The approach is rather general and applies to any anomalous Abelian gauge current. Anomalies are cancelled using either the Wess–Zumino mechanism with suitable Peccei–Quinn-like interactions and a Stückelberg axion, or by the Green–Schwarz mechanism. We compare predictions for the corresponding extra Z prime to anomaly-free realizations such as those involving $U(1)_{B-L}$. We identify the leading anomalous corrections to both channels, which contribute at higher orders, and compare them against the next-to-next-to-leading order (NNLO) QCD background. Anomalous effects in these inclusive observables are found to be small, below the size of the typical QCD corrections quantified by NNLO K -factors. Measurements at the LHC on the Z resonance in leptonproduction will be able to exclude a class of these models for variations of the cross section at the level of 4%, which is obtained at larger values of the anomalous coupling ($g_B > 1$). However, if they are not excluded, their anomalous nature is unlikely to be resolved with an inclusive NNLO analysis performed in these key processes.

© 2009 Elsevier B.V. All rights reserved.

* Corresponding author at: Dipartimento di Fisica, Università del Salento and INFN Sezione di Lecce, Via Arnesano, 73100 Lecce, Italy.

E-mail address: claudio.coriano@le.infn.it (C. Corianò).

1. Introduction

The study of anomalous gauge interactions at the LHC and at future linear colliders is for sure a difficult topic, but also an open possibility that deserves close theoretical and experimental attention. Hopefully, these studies will be able to establish if an additional anomalous extra Z' is present in the spectrum, introduced by an Abelian extension of the gauge structure of the Standard Model (SM), assuming that extra neutral currents will be found in the next several years of running of the LHC [1]. The interactions that we discuss are characterized by *genuine anomalous vertices* in which gauge anomalies cancel in some non-trivial way, not by a suitable (anomaly-free) charge assignment of the chiral fermion spectrum for each generation. The presence of an anomalous $U(1)$ in effective models derived from string theory is quite common, although in all the previous literature before [2] and [3–5] the phenomenological relevance of the anomalous $U(1)$ had not been worked out in any detail. In particular, the dynamics of the anomalous extra gauge interaction had been neglected, by invoking a decoupling of the anomalous sector on the assumption of a large mass of the extra gauge boson. Recent developments in the study of these models include their supersymmetric extensions [6] and their derivations as symplectic forms of supergravity [7,8]. Other interesting variants include the Stückelberg extensions considered in [9–11] which depart significantly from the Minimal Low Scale Orientifold Model (MLSOM) introduced in [2] and discussed below. Specifically these models are also characterized by the presence of two mechanisms of symmetry breaking (Higgs and Stückelberg) but do not share the anomalous structure. While a phenomenological study of Stückelberg axions is underway in a related work, here we focus our attention on the gauge sector, quantifying the rates for the detection of anomalous neutral currents at the LHC in some specific and very important channels. Related discussions of the GS mechanism based on the study of 4 fermion decay of the anomalous vertex can be found in [12].

Being leptonproduction the best way to search for extra neutral interactions, it is then obvious that the study of the anomalous vertices and of possible anomalous extra Z' should seriously consider the investigation of this process. We describe the modifications induced on Drell–Yan computed in the Standard Model (SM) starting from the description of some of the properties of the new anomalous vertices and of the corresponding 1-loop counterterms, before moving to the analysis of the corrections. These appear – both in the WZ and GS cases – in the relevant partonic channels at NNLO in the strong coupling constant ($O(\alpha_s^2)$). We perform several comparisons between anomalous and non-anomalous extra Z' models and quantify the differences with high accuracy.

Double prompt (direct) photons offer an interesting signal which is deprived of the fragmentation contributions especially at large values of their invariant mass Q , due to the steep falling of the photon fragmentation functions. In addition, photon isolation may provide an additional help in selecting those events coming from channels in which the contribution of the anomaly is more sizeable, such as gluon fusion. Also in this case we perform a detailed investigation of this sector. For direct photons, the anomaly appears in gluon fusion – at parton level – in a class of amplitudes which are characterized by two-triangles graphs – or BIM amplitudes – using the definitions of [13].

In both cases the quantification of the background needs extreme care, due to the small signal, and the investigation of the renormalization/factorization scale dependence of the predictions is of outmost importance. In particular, we consider all the sources of scale-dependence in the analysis, including those coming from the evolution of the parton densities (PDF's) which are just by themselves enough to overshadow the anomalous corrections. For this reason we have used

the program CANDIA in the evolution of the PDF's, which has been documented in [14]. The implementations of DY and DP are part of two programs CANDIA_{DY} and CANDIA_{AXION} for the study of the QCD background with the modifications induced by the anomalous signal. The QCD background in DP is computed using DIPHOX [15] and GAMMA2MC based on Ref. [16]. The NLO corrections to DP before the implementation of DIPHOX have been computed by Gordon and one of the authors back in 1995 [17] and implemented in a Monte Carlo based on the phase space slicing method. We present high precision estimates of the QCD background at NNLO, which is the order where, in these processes, the anomalous corrections start to appear. In principle, the size of these corrections, although small, cannot be classified as impossible to resolve at a collider, since both the size of the anomalous coupling and the mass of the extra gauge boson are unknown. In particular, the Z gauge boson has an anomalous component which is related to the specific charge assignment of a given model. While these charge assignments alone are not easily identifiable as being anomalous or not, they can however be excluded (or allowed) under some special conditions. For instance, in the brane model that we analyze, for a sizeable value of the anomalous coupling ($g_B \approx 1$) the variation induced on the Z resonance has a reduced overlap with the corresponding SM prediction, which points towards an exclusion of the same model for $g_B > 1$. However, since the PDF's need to be re-calibrated at higher evolution scales in the next few years, we prefer, on more conservative basis, to consider such models at such large couplings to be only marginally allowed and to wait for the experimental response. Coming to the anomalous corrections, although in DY these are found to be small, we find that they are comparable in size with the mass corrections due to heavy quarks in the hard scatterings, which have been computed before for the same process.

1.1. An anomalous extra Z'

The analysis of anomaly-free Abelian extensions of the SM that we will use in order to compare our results with the anomalous case, with our conventions, has been discussed in [38]. The numerical analysis presented here follows closely the choice of parameters presented in this previous work. In the presence of anomalous interactions we can use the same formalism with some appropriate changes. Since the effective Lagrangean of the class of the anomalous models that we are investigating includes both a Stückelberg and a two-Higgs doublet sector, the masses of the neutral gauge bosons are provided by a combination of these two mechanisms [18]. In this case we take as free parameters the Stückelberg mass M_1 and the anomalous coupling constant g_B , with $\tan \beta$ as in the remaining anomaly-free models. In the numerical study we have chosen v_{H_1} (vev of one of the two Higgs fields) of the order of the electroweak scale (≈ 246 GeV), allowing a small variability of M_Z within the experimental errors. In this case there is an allowed range of variability of $\tan \beta$, in the interval 10–40, which has been used to perform the analysis. The dependence of all the results on this parameter is rather weak, and for this reason we have fixed its value to $\tan \beta = 40$.

The value of M_1 is loosely constrained by the D-brane model in terms of suitable wrappings (n) of the 4-branes which define the charge embedding [19,20]. The charges are given in Table 3. Coming to the specific gauge structure of the model, we consider a complete $SU(3) \times SU(2) \times U(1)_Y \times U(1)_B$ symmetry, with $U(1)_B$ denoting the anomalous Abelian factor, in which anomaly cancellation is achieved via additional Wess–Zumino counterterms [5].

The mass-matrix in the neutral gauge sector is given by

$$\mathcal{L}_{\text{mass}} = (W_3, Y, B)\mathbf{M}^2 \begin{pmatrix} W_3 \\ Y \\ B \end{pmatrix},$$

where B is the Stückelberg field and the mass matrix is defined as

$$\mathbf{M}^2 = \frac{1}{4} \begin{pmatrix} g_2^2 v^2 & -g_2 g_Y v^2 & -g_2 x_B \\ -g_2 g_Y v^2 & g_Y^2 v^2 & g_Y x_B \\ -g_2 x_B & g_Y x_B & 2M_1^2 + N_{BB} \end{pmatrix} \quad (1)$$

with

$$N_{BB} = (q_u^{B2} v_u^2 + q_d^{B2} v_d^2) g_B^2, \quad x_B = (q_u^B v_u^2 + q_d^B v_d^2) g_B. \quad (2)$$

Here v_u and v_d denote the vevs of the two Higgs fields H_u, H_d while q_u^B and q_d^B are the Higgs charges under the extra anomalous $U(1)_B$. We have also defined $v = \sqrt{v_u^2 + v_d^2}$ and $g = \sqrt{g_2^2 + g_Y^2}$. The massless eigenvalue of the mass matrix is associated to the photon A_γ , while the two non-zero mass eigenvalues denote the masses of the Z and of the Z' vector bosons. These are given by

$$\begin{aligned} M_Z^2 &= \frac{1}{4} (2M_1^2 + g^2 v^2 + N_{BB} - \sqrt{(2M_1^2 - g^2 v^2 + N_{BB})^2 + 4g^2 x_B^2}) \\ &\simeq \frac{g^2 v^2}{2} - \frac{1}{M_1^2} \frac{g^2 x_B^2}{4} + \frac{1}{M_1^4} \frac{g^2 x_B^2}{8} (N_{BB} - g^2 v^2), \end{aligned} \quad (3)$$

$$\begin{aligned} M_{Z'}^2 &= \frac{1}{4} (2M_1^2 + g^2 v^2 + N_{BB} + \sqrt{(2M_1^2 - g^2 v^2 + N_{BB})^2 + 4g^2 x_B^2}) \\ &\simeq M_1^2 + \frac{N_{BB}}{2}. \end{aligned} \quad (4)$$

The mass of the Z gauge boson gets corrected by terms of the order v^2/M_1 , converging to the SM value as $M_1 \rightarrow \infty$, while the mass of the Z' gauge boson can grow large with M_1 . It is important to notice that the Stückelberg mechanism can be thought of as the low energy remnant of an extra Higgs whose radial fluctuations have been frozen and with the imaginary phase surviving at low energy as a CP-odd scalar [3,22]. The physical gauge fields can be obtained from the rotation matrix O^A

$$\begin{pmatrix} A_\gamma \\ Z \\ Z' \end{pmatrix} = O^A \begin{pmatrix} W_3 \\ A^Y \\ B \end{pmatrix} \quad (5)$$

which can be approximated at the first order in the mixing parameter ϵ_1 as

$$O^A \simeq \begin{pmatrix} \frac{g_Y}{g} & \frac{g_2}{g} & 0 \\ \frac{g_2}{g} + O(\epsilon_1^2) & -\frac{g_Y}{g} + O(\epsilon_1^2) & \frac{g}{2}\epsilon_1 \\ -\frac{g_2}{2}\epsilon_1 & \frac{g_Y}{2}\epsilon_1 & 1 + O(\epsilon_1^2) \end{pmatrix} \quad (6)$$

where ϵ_1 is defined by the expression

$$\epsilon_1 = \frac{x_B}{M_1^2}. \quad (7)$$

Table 1
Higgs charges in the Madrid model.

	Y	X_A	X_B
H_u	1/2	0	2
H_d	1/2	0	-2

Table 2
SM spectrum charges in the D -brane basis for the Madrid model.

	q_a	q_b	q_c	q_d
Q_L	1	-1	0	0
u_R	-1	0	1	0
d_R	-1	0	-1	0
L	0	-1	0	-1
e_R	0	0	-1	1
N_R	0	0	1	1

Table 3
Fermion spectrum charges in the Y -basis for the Madrid model [19].

	Q_L	u_R	d_R	L	e_R	N_R
q_Y	1/6	-2/3	1/3	-1/2	1	0
q_B	-1	0	0	-1	0	0

Concerning the charge assignments, the corresponding model is obtained from the intersection of 4 branes (a, b, c, d) with generators (q_a, q_b, q_c, q_d) which are rotated to the hypercharge basis, with an anomaly free hypercharge. The $U(1)_a$ and $U(1)_d$ symmetries are proportional to the baryon number and the lepton number respectively. The $U(1)_c$ symmetry can be considered as the third component of the right-handed weak isospin; the $U(1)_b$ is a PQ-like symmetry. A discussion of the construction can be found in [20] and [19]. One of the choice for these parameters is reported in Tables 1–3.

2. The GS and WZ vertices and gluon fusion

As we have mentioned above in the previous sections, the two available mechanisms that enforce at the level of the effective Lagrangean the cancellation of the anomalies involve either PQ-like (axion-like) interactions – in the WZ case – or the subtraction of the anomaly pole (for the GS case). In a related analysis [21] we have presented some of the main features of the two mechanisms taking as an example an axial (anomalous) version of QED to illustrate the cancellation of the anomaly in the two cases. In the GS case, the anomaly of a given diagram is removed by subtracting the longitudinal pole of the triangle amplitude in the chiral limit. We have stressed in [23] that the counterterm (the pole subtraction) amounts to the removal of one of the invariant amplitudes of the anomaly vertex (the longitudinal component) and corresponds to a vertex re-definition.

The procedure is exemplified in Fig. 1 where we show the triangle anomaly and the pole counterterm which is subtracted from the first amplitude. The combination of the two contributions defines the GS vertex, which is made of purely transverse components in the chiral limit [21] and satisfies an ordinary Ward identity. Notice that the vertex does not require an axion as an

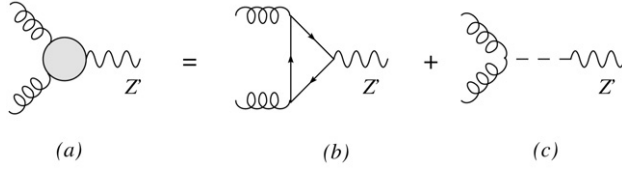


Fig. 1. A gauge invariant GS vertex of the AVV type, composed of an AVV triangle and a single counterterm of the Dolgov–Zakharov form.

asymptotic state in the related S-matrix; for a non-zero fermion mass in the triangle diagram, the vertex satisfies a broken Ward identity. We now proceed and summarize some of these properties, working in the $m_f = 0$ limit (i.e. the chiral limit).

Processes such as $gg \rightarrow \gamma\gamma$, mediated by an anomalous gauge boson Z' , can be expressed in a simplified form in which only the longitudinal component of the anomaly appears. We therefore set $k_1^2 = k_2^2 = 0$ and $m_f = 0$, which are the correct kinematical conditions to obtain the anomaly pole, necessary for a parton model (factorized) description of the cross section in a pp collision at the LHC, where the initial state of the partonic hard-scatterings are on-shell.

We start from the Rosenberg form of the AVV amplitude, which is given by

$$T^{\lambda\mu\nu} = A_1 \varepsilon[k_1, \lambda, \mu, \nu] + A_2 \varepsilon[k_2, \lambda, \mu, \nu] + A_3 k_1^\mu \varepsilon[k_1, k_2, \nu, \lambda] + A_4 k_2^\mu \varepsilon[k_1, k_2, \nu, \lambda] + A_5 k_1^\nu \varepsilon[k_1, k_2, \mu, \lambda] + A_6 k_2^\nu \varepsilon[k_1, k_2, \mu, \lambda], \quad (8)$$

where the two external outgoing momenta are k_1^μ and k_2^ν , while the incoming momentum is $k^\lambda = (k_1 + k_2)^\lambda$. Imposing the Ward identities to bring all the anomaly on the axial-vector vertex, we obtain the usual conditions

$$\begin{aligned} A_1 &= k_2^2 A_6 + k_1 \cdot k_2 A_5, \\ A_2 &= k_1^2 A_3 + k_1 \cdot k_2 A_4, \\ A_3(k_1, k_2) &= -A_6(k_1, k_2), \\ A_4(k_1, k_2) &= -A_5(k_1, k_2), \end{aligned} \quad (9)$$

where the invariant amplitudes A_3, \dots, A_6 are free from kinematical singularities for off-shell external lines. We set $k^2 = (k_1 + k_2)^2 = s$. As we have mentioned, in the parton model we take the initial gluons to be on-shell, while the hadronic cross section is obtained by convoluting the hard scattering given above (corrected by a color factor) with the PDF's. The amplitude simplifies drastically in this case using repeatedly the Schouten relation, and takes the form (see [24])

$$T^{\lambda\mu\nu} = A_6 k^\lambda \varepsilon[k_1, k_2, \nu, \mu] + (A_4 + A_6) (k_2^\nu \varepsilon[k_1, k_2, \mu, \lambda] - k_1^\mu \varepsilon[k_1, k_2, \nu, \lambda]), \quad (10)$$

in which the second piece drops off for physical on-shell photon/gluon lines, leaving only a single invariant amplitude to contribute to the final result

$$T^{\lambda\mu\nu} = A_6^f(s) (k_1 + k_2)^\lambda \varepsilon[k_1, k_2, \nu, \mu] \quad (11)$$

where

$$A_6^f(s) = \frac{1}{2\pi^2 s} \left(1 + \frac{m_f^2}{s} \log^2 \frac{\rho_f + 1}{\rho_f - 1} \right), \quad \rho_f = \sqrt{1 - 4 \frac{m_f^2}{s}}, \quad s < 0. \quad (12)$$

The anomaly pole is given by the first term of Eq. (10)

$$T_c^{\lambda\mu\nu} \equiv \frac{1}{2\pi^2 s} (k_1 + k_2)^\lambda \varepsilon[k_1, k_2, \nu, \mu]. \quad (13)$$

The logarithmic functions in the expression above are continued in the following way in the various region

$$\begin{aligned} 0 < s < 4m_f^2: \\ \rho_f \rightarrow i\sqrt{-\rho_f^2}; \quad \frac{1}{2} \log\left(\frac{\rho_f + 1}{\rho_f - 1}\right) &\rightarrow -i \arctan \frac{\sqrt{s}}{\sqrt{4m_f^2 - s}}, \\ s > 4m_f^2 > 0: \\ \sqrt{-\rho_f^2} \rightarrow -i\rho_f; \quad \arctan \frac{1}{\sqrt{-\rho_f^2}} &\rightarrow \frac{\pi}{2} + \frac{i}{2} \log\left(\frac{\sqrt{s - 4m_f^2} + \sqrt{s}}{\sqrt{s} - \sqrt{s - 4m_f^2}}\right). \end{aligned} \quad (14)$$

Notice that the surviving amplitude A_6 multiplies a longitudinal momentum exchange and, as discussed in the literature on the chiral anomaly in QCD [24,25], is characterized by a massless pole in s , which is the anomaly pole, as one can clearly conclude from Eq. (12). This equation shows also how chiral symmetry breaking effects appear in this amplitude at this special kinematical point by the m_f terms.

The subtraction of the anomaly pole is shown in Fig. 1 and is represented by diagram (c). The combination of diagrams (b) and (c) defines the GS vertex of the theory [21], with diagram (c) described by Eq. (13) ($-T_c$). Therefore, in the AVV case, it is explicitly given by

$$\Delta_{\text{AVV}}^{\lambda\mu\nu\text{GS}}(k, k_1, k_2) = \Delta_{\text{AVV}}^{\lambda\mu\nu}(k, k_1, k_2) + C_{\text{AVV}}^{\lambda\mu\nu}(k, k_1, k_2) \quad (15)$$

where we have denoted with Δ_{AVV} the anomaly diagram and the GS counterterm that corresponds to the exchange of the massless pole takes the following form in momentum space in the AVV case

$$C_{\text{AVV}}^{\lambda\mu\nu}(k, k_1, k_2) = -\frac{a_n}{k^2} k^\lambda \varepsilon[\mu, \nu, k_1, k_2], \quad (16)$$

where a_n is the anomaly. We will refer to this expression as to the Dolgov–Zakharov (or DZ) counterterm [25].

It is easily verified that in the massless fermion limit and for on-shell gluon lines, the GS vertex is trivially vanishing by construction. In general, for any asymmetric configuration of the external lines in the vertex, even in the massless limit, the vertex has non-zero transverse components [26, 27]. The expression is well known [27,28] in the chiral limit and has been shown to satisfy the Adler–Bardeen theorem [27].

2.1. BIM amplitudes

In our analysis we encounter a class of amplitudes (BIM) [13] which are characterized by two anomaly vertices connected by an s -channel exchange of the anomalous gauge boson. These amplitudes grow quadratically with the energy and are not eliminated by the exchange of a Stückelberg pseudoscalar. The amplitude appears in the gluon fusion sector in the WZ case. In the SM a similar graph contributes only if heavy fermions run in the loop. Obviously, this

contribution would be identically vanishing if all the fermions of a given generation would be mass-degenerate.

Notice that a BIM amplitude is non-resonant and can grow beyond the unitarity limit. In the massless fermion case, its expression is given by the Dolgov–Zakharov limit of the anomaly amplitude (Eqs. (11) and (12), with $m_f = 0$), which appears both in the production mechanism of the extra Z' ($gg \rightarrow Z'$), where the Z' in the s -channel is virtual, and in its decay into two photons. The disappearance of the s -channel resonance, in this amplitude, is a consequence of the anomaly, as one can show rather simply [13]. The explicit expression of the BIM amplitude is given by

$$\begin{aligned}
 A_{\text{BIM}} &= \frac{a_n}{k^2} k^\lambda \varepsilon[\mu, \nu, k_1, k_2] \frac{-i}{k^2 - M^2} \left(g^{\lambda\lambda'} - \frac{k^\lambda k^{\lambda'}}{M^2} \right) \frac{a_n}{k^2} (-k^{\lambda'}) \varepsilon[\mu', \nu', k'_1, k'_2] \\
 &= \frac{a_n}{k^2} \varepsilon[\mu, \nu, k_1, k_2] \frac{-i}{k^2 - M^2} \frac{k^{\lambda'} (M^2 - k^2)}{M^2} \frac{a_n}{k^2} (-k^{\lambda'}) \varepsilon[\mu', \nu', k'_1, k'_2] \\
 &= \frac{a_n}{k^2} \varepsilon[\mu, \nu, k_1, k_2] \left(\frac{-ik^2}{M^2} \right) \frac{a_n}{k^2} \varepsilon[\mu', \nu', k'_1, k'_2] \\
 &= -\frac{a_n}{M} \varepsilon[\mu, \nu, k_1, k_2] \frac{i}{k^2} \frac{a_n}{M} \varepsilon[\mu', \nu', k'_1, k'_2] \tag{17}
 \end{aligned}$$

where M denotes, generically, the mass of the anomalous gauge boson in the s -channel. If we multiply this amplitude by the external polarizators of the photons, square it and perform the usual averages, one finds that it grows quadratically with energy. Therefore, in general one encounters, for models of these types, a unitarity bound, as discussed in [13]. The impact of these amplitudes on the selected cross sections, at the LHC energy, will be quantified below.

3. Invariant mass distributions in Drell–Yan

Our NNLO analysis of the invariant mass distributions for lepton pair production, for the computation of the QCD sectors, is based on the hard scatterings of [29], and the NNLO evolution of the parton distributions (PDF’s) has been obtained with CANDIA [14]. The anomalous corrections to the invariant mass distributions have been evaluated separately, since at NNLO they appear in DY in the interference with the lowest order graph, and have been added to the standard QCD background. It is important to recall that lepton pair production at low Q via Drell–Yan is sensitive to the PDF’s at small- x values, while in the high mass region this process is essential in the search of additional neutral currents. In our analysis we have selected a mass of 1 TeV for the extra gauge boson and analyzed the signal and the background both on the peaks of the Z and of the new resonance.

At hadron level the colour-averaged inclusive differential cross section for the reaction $H_1 + H_2 \rightarrow l_1 + l_2 + X$, is given by the expression [29]

$$\frac{d\sigma}{dQ^2} = \tau \sigma_{\mathcal{Z}}(Q^2, M_{\mathcal{Z}}^2) W_{\mathcal{Z}}(\tau, Q^2), \quad \tau = \frac{Q^2}{S}, \tag{18}$$

where $\mathcal{Z} \equiv Z, Z'$ is the point-like cross section and all the information from the hadronic initial state is contained in the PDF’s. The hadronic structure function $W_{\mathcal{Z}}(\tau, Q^2)$ is given by a con-

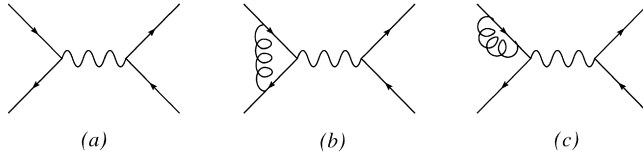


Fig. 2. $q\bar{q} \rightarrow Z, Z' \rightarrow l^+l^-$ at LO and NLO (virtual corrections).

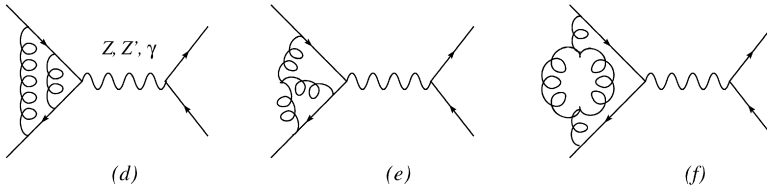


Fig. 3. $q\bar{q} \rightarrow Z, Z' \rightarrow l^+l^-$ at NNLO (virtual corrections).

volution product between the parton luminosities $\Phi_{ij}(x, \mu_R^2, \mu_F^2)$ and the Wilson coefficients $\Delta_{ij}(x, Q^2, \mu_R^2, \mu_F^2)$

$$W_Z(\tau, Q^2, \mu_R^2, \mu_F^2) = \sum_{i,j} \int_{\tau}^1 \frac{dx}{x} \Phi_{ij}(x, \mu_R^2, \mu_F^2) \Delta_{ij}\left(\frac{\tau}{x}, Q^2, \mu_F^2\right), \tag{19}$$

where i and j denote the various partons and where the luminosities are given by

$$\Phi_{ij}(x, \mu_R^2, \mu_F^2) = \int_x^1 \frac{dy}{y} f_i(y, \mu_R^2, \mu_F^2) f_j\left(\frac{x}{y}, \mu_R^2, \mu_F^2\right) \equiv [f_i \otimes f_j](x, \mu_R^2, \mu_F^2). \tag{20}$$

The Wilson coefficients (hard scatterings) depend on both the factorization (μ_F) and renormalization scales (μ_R), formally expanded in the strong coupling α_s as

$$\Delta_{ij}(x, Q^2, \mu_F^2) = \sum_{n=0}^{\infty} \alpha_s^n(\mu_R^2) \Delta_{ij}^{(n)}(x, Q^2, \mu_F^2, \mu_R^2). \tag{21}$$

We will vary μ_F and μ_R independently in order to determine the sensitivity of the result on their variations and their optimal choice. Coming to illustrate the contributions included in our analysis, these are shown in some representative graphs. The complete NNLO expressions of the hard scatterings and the corresponding Feynman diagrams can be found in [29]. We briefly discuss the various contributions in order to identify the new anomaly graphs.

• SM QCD contributions

We show in Fig. 2 the leading $O(\alpha_w)$ and some typical next-to-leading order $O(\alpha_w\alpha_s)$ (LO, NLO) contributions to the process in the annihilation channel (virtual corrections). Examples of higher order virtual corrections included in the hard scatterings are shown in Fig. 3, which are of $O(\alpha_s^2\alpha_w)$, while the corresponding real emissions, integrated over the final state gluons, are shown in Fig. 4 at NLO (graph (g)) and NNLO (graphs (h) and (i)).

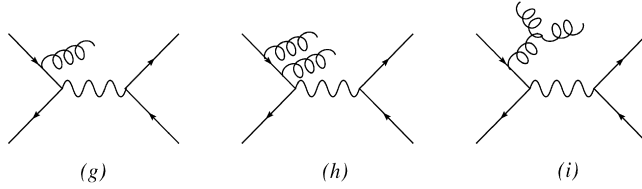


Fig. 4. $q\bar{q} \rightarrow Z, Z' \rightarrow l^+l^-$ with real corrections at NLO (g) and at NNLO (h), (i).

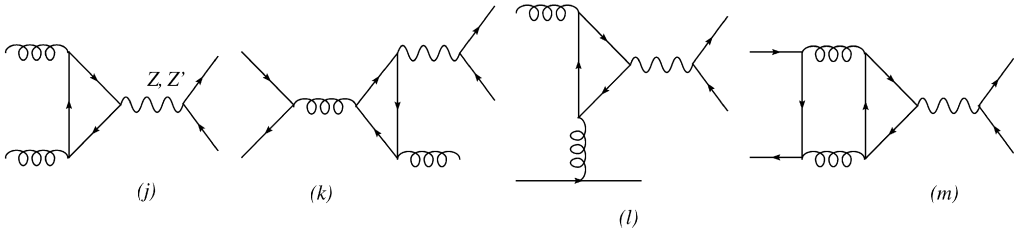


Fig. 5. Anomalous contributions to lepton production mediated by a Z' in the gg , $q\bar{q}$ and qg sectors.

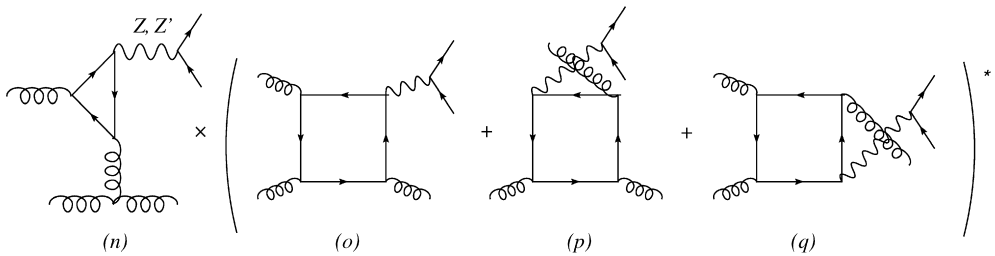


Fig. 6. Anomalous contributions to lepton production in the gg sector mediated by an anomalous Z' at higher perturbative orders.

• *Anomalous corrections*

We have shown in Figs. 5, 6 the leading anomalous corrections to lepton production. At $O(\alpha_s^2\alpha_w^2)$ there is a first contribution coming from the square of graph (j) a second contribution coming from the interference between graph (k) of this figure and graph (g) of Fig. 4; a third contribution coming from the interference between graph (l) of this figure and graph (i) of Fig. 4, which involve the qg sector, and the interference between graph (m) of this figure and graph (a) of Fig. 2 in the $q\bar{q}$ sector. The analogous contributions in the WZ and GS cases are obtained by replacing the triangle graph with the GS vertex, as in Fig. 1. Notice that in the WZ case the anomaly pole is automatically cancelled by the Ward identity on the lepton pair of the final state, if the two leptons are taken to be massless at high energy, as is the case. Then, the only new contributions from the anomaly vertex that survive are those related to the transverse component of this vertex. This is an example, as we have discussed in [21], of a “harmless” anomaly vertex. A similar situation occurs whenever there is no coupling of the longitudinal component of the anomaly to the (transverse) external leptonic current.

3.1. Precision studies on the Z resonance

The quantification of the corrections due to anomalous Abelian gauge structures in DY requires very high precision, being these of a rather high order. For this reason we have to identify all the sources of indeterminations in QCD which come from the factorization/renormalization scale dependence of the cross section, keeping into account the dependence on μ_F and μ_R both in the DGLAP evolution and in the hard scatterings. The set-up of our analysis is similar to that used for a study of the NNLO DGLAP evolution in previous works [30,31], where the study has covered every source of theoretical error, including the one related to the various possible resummations of the DGLAP solution, which is about 2–3% in DY and would be sufficient to swamp away any measurable deviation due to new physics at the LHC.

We will now briefly summarize the results for the new contributions in DY, starting from the non-anomalous ones.

In the $q\bar{q}$ sector we have two contributions involving triangle fermion loops see Fig. 5(k), (m). The one depicted in Fig. 5(m) is a two-loop virtual correction with a Z or a Z' boson in the final state, while in Fig. 5(k) we have a real emission of a gluon in the final state which is integrated out. The first contribution has been calculated in [32–35],

$$\begin{aligned} \Delta_{q\bar{q}}^V(x, Q^2, \mu_F^2, m^2) &= \delta(1-x) a_q^{Z'} a_{\bar{q}}^{Z'} C_F T_f \frac{1}{2} \left(\frac{\alpha_s}{\pi} \right)^2 [\theta(Q^2 - 4m^2) G_1(m^2/Q^2) \\ &\quad + \theta(4m^2 - Q^2) G_2(m^2/Q^2)] \end{aligned} \quad (22)$$

where C_F and T_f are the color factors, $q = u, d, c, s$, $Q = t, b$ and m the mass of the heavy flavors, while in the massless limit the functions G_1 and G_2 are given by

$$\begin{aligned} G_1(m=0) &= 3 \log\left(\frac{Q^2}{\mu_R^2}\right) - 9 + 2\zeta(2), \\ G_2(m=0) &= 0 \end{aligned} \quad (23)$$

and Q represents the invariant mass of the system. The contribution of Fig. 5(k) in the massless limit is given by

$$\begin{aligned} \Delta_{q\bar{q}}^R(x, Q^2, \mu_F^2, m=0) &= a_q^{Z'} a_{\bar{q}}^{Z'} C_F T_f^2 \frac{1}{2} \left(\frac{\alpha_s}{\pi} \right)^2 \times \left\{ \frac{(1+x)}{(1-x)_+} [-2 + 2x(1 - \log(x))] \right\}, \end{aligned} \quad (24)$$

while in the qg sector we have the contribution shown in Fig. 5(l) which is given by

$$\begin{aligned} \Delta_{qg}(x, Q^2, \mu_F^2, m^2) &= a_q^{Z'} a_{\bar{q}}^{Z'} T_f^2 \frac{1}{2} \left(\frac{\alpha_s}{\pi} \right)^2 \times [\theta(Q^2 - 4m^2) H_1(x, Q^2, m^2) \\ &\quad + \theta(4m^2 - Q^2) H_2(x, Q^2, m^2)] \end{aligned} \quad (25)$$

with the massless limit of $H_1(x, Q^2, m^2)$ given by

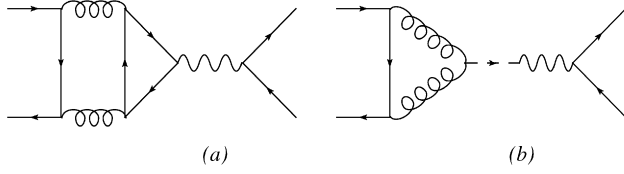


Fig. 7. GS mechanism: anomalous contribution and counterterm for the $q\bar{q}$ scattering sector.

$$\begin{aligned}
 H_1(x, Q^2, m = 0) = & 2x \left[\log\left(\frac{1}{x}\right) \log\left(\frac{1}{x} - 1\right) + \text{Li}_2\left(1 - \frac{1}{x}\right) \right] \\
 & + 2\left(1 - \frac{1}{x}\right) \left[1 - 2x \log\left(\frac{1}{x}\right) \right].
 \end{aligned} \tag{26}$$

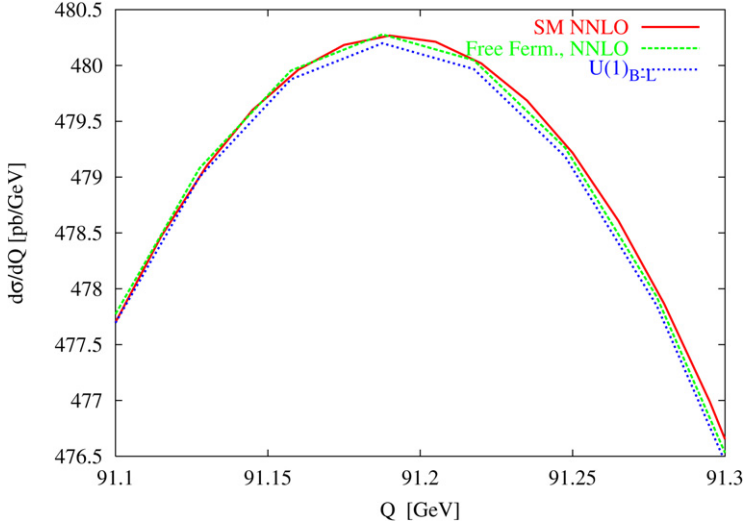
Separating the anomaly-free from the anomalous contributions, the factorization formula for the invariant mass distribution in DY is given by

$$\begin{aligned}
 \frac{d\sigma}{dQ^2} = & \tau \sigma_{\mathcal{Z}}(Q^2, M_{\mathcal{Z}}^2) \{ W_{\mathcal{Z}}(\tau, Q^2) + W_{\mathcal{Z}}^{\text{anom}}(\tau, Q^2) \}, \\
 W_{\mathcal{Z}}^{\text{anom}}(\tau, Q^2) = & \sum_{i,j} \int_{\tau}^1 \frac{dx}{x} \Phi_{ij}(x, \mu_R^2, \mu_F^2) \Delta_{ij}^{\text{anom}}\left(\frac{\tau}{x}, Q^2, \mu_F^2\right), \\
 \Delta_{ij}^{\text{anom}}(x, Q^2, \mu_F^2) = & \Delta_{q\bar{q}}^V(x, Q^2, \mu_F^2, m = 0) + \Delta_{q\bar{q}}^R(x, Q^2, \mu_F^2, m = 0) \\
 & + \Delta_{qg}(x, Q^2, \mu_F^2, m = 0)
 \end{aligned} \tag{27}$$

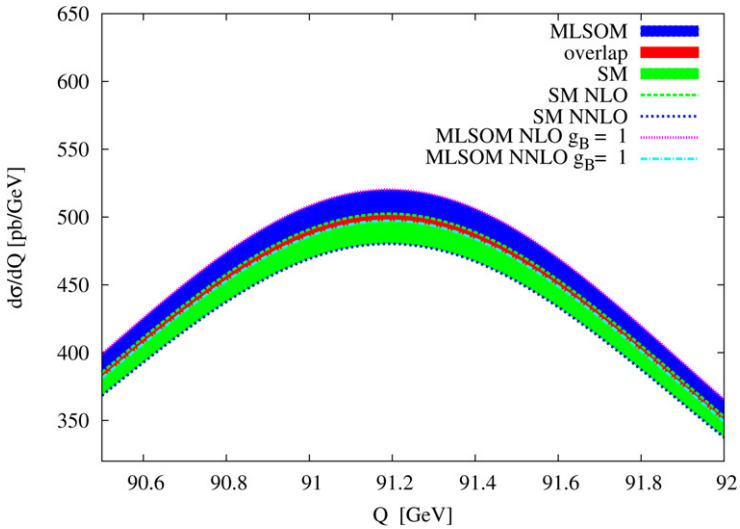
where \mathcal{Z} stays for Z, Z' and that we will be using in our numerical analysis below. In Fig. 7 we have illustrated one of the anomalous contributions and its counterterm in the $q\bar{q}$ sector for the GS case.

3.2. Di-lepton production: Numerical results

We have used the MRST-2001 set of PDF's given in [36] and [37]. We start by showing in Fig. 8 various zooms of the differential cross section on the peak of the Z – for all the models – both at NLO and at NNLO. We have kept the factorization and renormalization scales coincident and equal to Q , while the mass of the extra Z' has been chosen around 1 TeV. The anomaly-free models, from the SM to the three Abelian extensions that we have considered (free fermionic [38] and $U(1)_{B-L}$ [39] in Fig. 8, while $U(1)_{q+u}$ appears in Table 5) show that the cross section is more enhanced for the MLSOM, illustrated in Fig. 8(c). The plots show a sizeable difference (at a 3.5% level) between the anomalous and all the remaining anomaly-free models. From Fig. 8(c) it is clear that the variation of the SM cross section from NLO to NNLO has an overlap with the corresponding variation for the MLSOM. Notice that given this intersection between the two bands of variations, it is clear that it is not possible to exclude this model at such value of the coupling, although future analysis, based on new sets of PDF's calibrated at larger energy at the LHC, may be able to do so. It is important to stress that these variations are due to the specific charge assignments of the model and not to the presence of anomalous contributions on the Z resonance. The reason for this is that even at NLO, where the anomalous corrections are absent, these discrepancies with the SM are already present. It is also important to stress that $g_B = 1$ is probably a large value for an extra Abelian coupling. For these reasons the model is



(a) SM vs anomaly-free models at NNLO



(b) Overlaps at NLO/NNLO

Fig. 8. Zoom on the Z resonance for anomalous Drell–Yan in the $\mu_F = \mu_R = Q$ at NLO/NNLO for all the models.

not (currently) completely excluded by precision LEP data, but might be excluded in the future at least for such larger value of the coupling, since the dependence of the shape of the peak on this parameter is significant.

Moving from NLO to NNLO the cross section is reduced in correspondence of the Z_0 peak. Defining the K -factor

$$\frac{\sigma_{\text{NNLO}} - \sigma_{\text{NLO}}}{\sigma_{\text{NLO}}} \equiv K_{\text{NLO}} \tag{28}$$

Table 4

Invariant mass distributions at NNLO for the MLSOM and the SM around the peak of the Z . The mass of the anomalous extra Z' is taken to be 1 TeV with $\mu_F = \mu_R = Q$.

$d\sigma^{\text{nnlo}}/dQ$ [pb/GeV] for the MLSOM with $M_1 = 1$ TeV, $\tan\beta = 40$, CANDIA evol.					
Q [GeV]	$g_B = 0.1$	$g_B = 0.36$	$g_B = 0.65$	$g_B = 1$	$\sigma_{\text{nnlo}}^{\text{SM}}(Q)$
90.50	$3.684 \times 10^{+2}$	$3.6997 \times 10^{+2}$	$3.7374 \times 10^{+2}$	$3.8132 \times 10^{+2}$	$3.6835 \times 10^{+2}$
90.54	$3.7956 \times 10^{+2}$	$3.8112 \times 10^{+2}$	$3.8500 \times 10^{+2}$	$3.9282 \times 10^{+2}$	$3.7945 \times 10^{+2}$
90.59	$3.9054 \times 10^{+2}$	$3.9215 \times 10^{+2}$	$3.9615 \times 10^{+2}$	$4.0419 \times 10^{+2}$	$3.9043 \times 10^{+2}$
90.63	$4.0132 \times 10^{+2}$	$4.0298 \times 10^{+2}$	$4.0708 \times 10^{+2}$	$4.1535 \times 10^{+2}$	$4.0121 \times 10^{+2}$
90.68	$4.1180 \times 10^{+2}$	$4.1351 \times 10^{+2}$	$4.1772 \times 10^{+2}$	$4.2621 \times 10^{+2}$	$4.1169 \times 10^{+2}$
90.99	$4.6879 \times 10^{+2}$	$4.7073 \times 10^{+2}$	$4.7554 \times 10^{+2}$	$4.8523 \times 10^{+2}$	$4.6866 \times 10^{+2}$
91.187	$4.8040 \times 10^{+2}$	$4.8239 \times 10^{+2}$	$4.8733 \times 10^{+2}$	$4.9727 \times 10^{+2}$	$4.8027 \times 10^{+2}$
91.25	$4.7935 \times 10^{+2}$	$4.8134 \times 10^{+2}$	$4.8627 \times 10^{+2}$	$4.9619 \times 10^{+2}$	$4.7922 \times 10^{+2}$
91.56	$4.4076 \times 10^{+2}$	$4.4259 \times 10^{+2}$	$4.4713 \times 10^{+2}$	$4.5628 \times 10^{+2}$	$4.4064 \times 10^{+2}$
91.77	$3.9371 \times 10^{+2}$	$3.9535 \times 10^{+2}$	$3.9941 \times 10^{+2}$	$4.0759 \times 10^{+2}$	$3.9360 \times 10^{+2}$
92.0	$3.3750 \times 10^{+2}$	$3.3891 \times 10^{+2}$	$3.4239 \times 10^{+2}$	$3.4942 \times 10^{+2}$	$3.3741 \times 10^{+2}$

in the case of the MLSOM this factor indicates a reduction of about 4% on the peak and can be attributed to the NNLO terms in the DGLAP evolution, rather than to the NNLO corrections to the hard scatterings. This point can be explored numerically by the (order) variation [30,40]

$$\Delta\sigma \sim \Delta\hat{\sigma} \otimes \phi + \hat{\sigma} \otimes \Delta\phi,$$

$$\Delta\sigma \equiv |\sigma_{\text{NNLO}} - \sigma_{\text{NLO}}| \quad (29)$$

which measures the “error” change in the hadronic cross section σ going from NLO to NNLO ($\Delta\sigma$) in terms of the analogous changes in the hard scatterings ($\Delta\hat{\sigma}$) and parton luminosities ($\Delta\phi$). The dominance of the first or the second term on the rhs of Eq. (29) is an indication of the dominance of the hard scatterings or of the evolution in moving from lower to higher order. We show in Table 4 numerical results for the NNLO cross section. Differences in the resonance region of this size can be considered marginally relevant for the identification of anomalous components in this observables. In fact, in [30] a high precision study of this distributions on the same peak (in the SM case) shows that the total theoretical error is reasonably below the 4% level and can decrease at 1.5–2% level when enough statistics will allow to reduce the experimental errors on the PDF’s. It is then obvious that the isolation/identification of a specific model – whether anomalous or not – appears to be rather difficult from the measurement of a single observable even with very high statistics, such as the Z resonance.

The evolution of the PDF’s has been performed with CANDIA [14] which allows independent variations of μ_F and μ_R in the initial state. This analysis is shown in Fig. 9, where we vary μ_F up to $2Q$, while we have taken $1/2\mu_F \leq \mu_R \leq 2\mu_F$. We observe that by increasing both scales there is an enhancement in the result and this is due to the logarithms $\ln\mu_R^2/\mu_F^2$ and $\ln Q^2/\mu_F^2$, contained in the hard scatterings. The scale variations induce changes of about 4% in the SM case at NNLO and about 3.5% in the MLSOM on the peak of the Z . Notice that the variations are not symmetric as we vary the scales and the percentual changes refer to the maximum variability. This typical scale dependence is universal for all the studies presented so far on the peak of the Z and is a limitation of the parton model prediction. After a large data taking, optimal choices for the PDF’s and for μ_R and μ_F will allow a considerable reduction of this indetermination. In Fig. 9(b) we repeat the same analysis, for the same center of mass

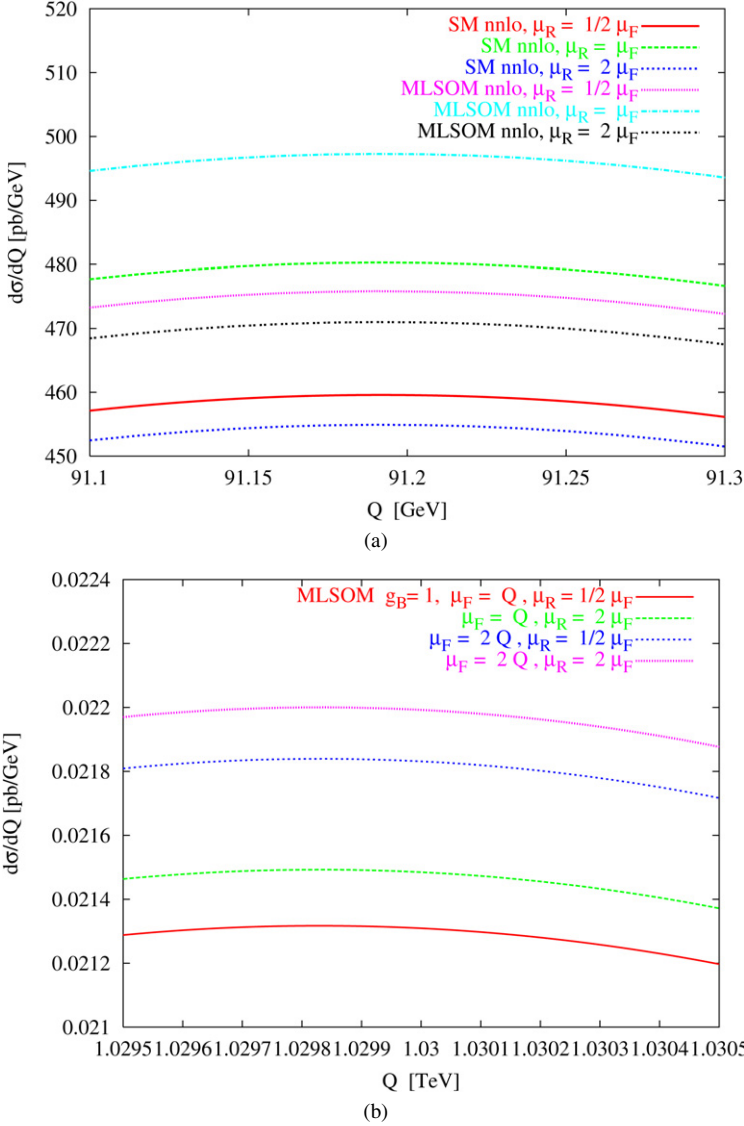


Fig. 9. Zoom on the Z resonance for anomalous Drell–Yan obtained by varying the factorization and the renormalization scales at NNLO for the SM and the MLSOM. Results are shown for $Q \sim M_{Z_0}$ GeV (a) and 1 TeV (b) both for $\sqrt{s} = 14$ TeV.

energy, this time for $Q \sim 1$ TeV, on the Z' resonance in the MLSOM, for a sizeable coupling of the anomalous gauge boson, $g_B = 1$. Compared to the value on the Z peak, the reduction of the cross section is by a factor of 2×10^4 . Also in this interval the variation of the differential cross section with the two scales is around 3%. We have added a table (Table 5) in which we show results for the total cross sections for the various models at the Z peak. In the first line of each column we show the results for the total cross section in [fb], in the 2nd line the total width $\Gamma_{Z'}$, expressed in GeV and in the 3rd line the observable $\sigma_{\text{tot}} \times \text{BR}(Z' \rightarrow l\bar{l})$, where

Table 5

Total cross sections, widths and $\sigma_{\text{tot}} \times \text{BR}(Z' \rightarrow l\bar{l})$, where $\text{BR}(Z' \rightarrow l\bar{l}) = \Gamma_{Z' \rightarrow l\bar{l}}/\Gamma_{Z'}$, for the MLSOM and three anomaly-free extensions of the SM; they are all shown as functions of the coupling constant.

$\sigma_{\text{tot}}^{\text{nnlo}}$ [fb], $\sqrt{S} = 14$ TeV, $M_1 = 1$ TeV, $\tan\beta = 40$				
g_B	MLSOM	$U(1)_{B-L}$	$U(1)_{q+u}$	Free Ferm.
0.1	5.982	3.575	2.701	1.274
	0.173	0.133	0.177	0.122
	0.277	0.445	0.252	0.017
0.36	106.674	105.567	53.410	42.872
	2.248	1.733	2.308	1.583
	4.937	13.138	4.991	0.586
0.65	240.484	143.455	108.344	51.155
	7.396	5.700	7.592	5.205
	11.127	17.853	10.124	0.699
1	532.719	317.328	239.401	113.453
	17.810	13.720	18.274	12.530
	24.639	39.491	22.370	1.550

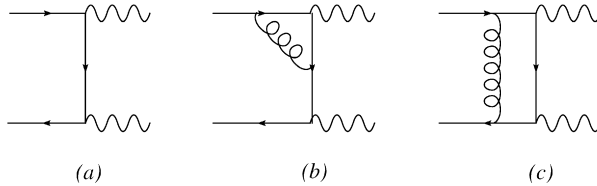


Fig. 10. $q\bar{q}$ sector for the process $q\bar{q} \rightarrow \gamma\gamma$ including virtual corrections at LO (a) and NLO (b), (c).

$\text{BR}(Z' \rightarrow l\bar{l}) = \Gamma_{Z' \rightarrow l\bar{l}}/\Gamma_{Z'}$. These quantities refer to the value of the coupling constant g_B listed in the first column.

4. Direct photons with GS and WZ interactions

The analysis of $pp \rightarrow \gamma\gamma$ proceeds similarly to the DY case, with a numerical investigation of the background and of the anomalous signal at parton level. We start classifying the strong/weak interference effects that control the various sectors of the process and then identify the leading contributions due to the presence of anomaly diagrams.

We show in Fig. 10 a partial list of the various background contributions to the DP channel in pp collisions. Notice that, due to the anomaly, the 2-photon signal is non-resonant, even in the presence of an s -channel exchange.

We show the leading order (LO) contribution in diagram (a) with some of the typical virtual corrections included in (b) and (c). These involve the $q\bar{q}$ sector giving a cross section of the form

$$\sigma_{q\bar{q}} = \alpha_{em}^2 (c_1 + c_2\alpha_s). \tag{30}$$

These corrections are the NLO ones in this channel. The infrared safety of the process is guaranteed at the same perturbative order by the real emissions in Fig. 11 with an integrated gluon in the final state, which are also of $O(\alpha_{em}^2\alpha_s)$.

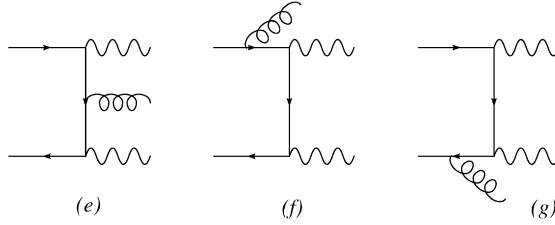


Fig. 11. Real emissions for $q\bar{q} \rightarrow \gamma\gamma$ at NLO.

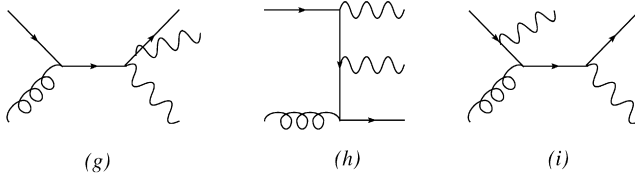


Fig. 12. gg sector for the process $qg \rightarrow \gamma\gamma$.

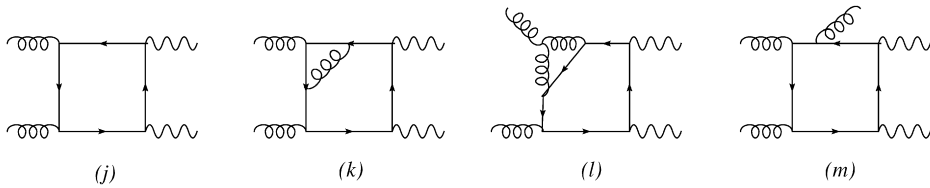


Fig. 13. gg sector for the process $gg \rightarrow \gamma\gamma$ with virtual and real radiative corrections.

A second sector is the qg one, which is shown in Fig. 12, also of the same order ($O(\alpha_s\alpha_{em})$). These corrections are diagrammatically the NLO ones. In general, the NLO prediction for this process are improved by adding a part of the NNLO (or $O(\alpha_{em}^2\alpha_s^2)$) contributions, such as the box contribution (j) of the gg sector which is of higher order ($O(\alpha_{em}^2\alpha_s^2)$) in α_s , the reason being that these contributions have been shown to be sizeable and comparable with the genuine NLO ones. All these corrections have been computed long ago [17] and implemented independently in a complete Monte Carlo in [15,41] with a more general inclusion of the fragmentation. More recently, other NNLO contributions have been added to the process, such as those involving the gg sector through $O(\alpha_{em}^2\alpha_s^3)$,

$$\sigma_{gg} = \alpha_{em}^2 (d_1\alpha_s^2 + d_2\alpha_s^3), \tag{31}$$

shown in graphs (k), (l), (m). The other sectors have not yet been computed with the same accuracy, for instance in the qq and $q\bar{q}$ channels they involve 2 to 4 emission amplitudes which need to be integrated over 2 gluons. For instance, graph (m) is a real emission in σ_{gg} which is needed to cancel the infrared/collinear singularities of the virtual ones at the same order.

The anomalous contributions are shown in Figs. 14–17 and 18.¹ The additional contributions in the s -channel that accompany this amplitude are shown in Fig. 19. The exchange of a massive axion (Fig. 19(b)), due to a mismatch between the coupling and the parametric dependence

¹ As stated in the previous sections, the diagram in Fig. 17 vanishes because of a Ward identity.

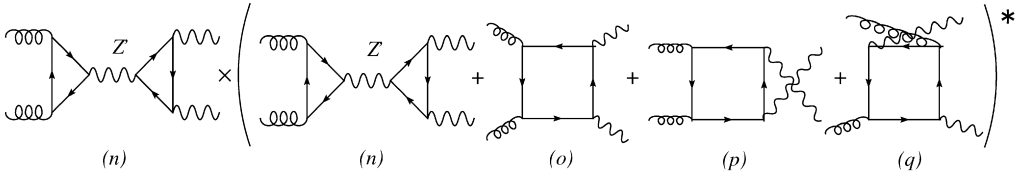


Fig. 14. Anomalous contributions for $gg \rightarrow \gamma\gamma$ involving the BIM amplitude and its interference with the box graphs.

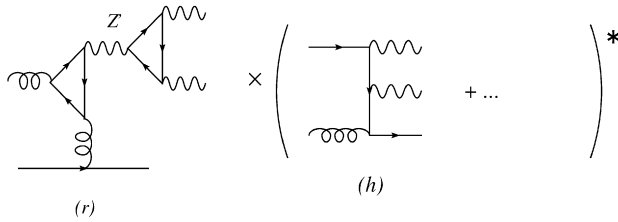


Fig. 15. Total amplitude for $qg \rightarrow \gamma\gamma q$.

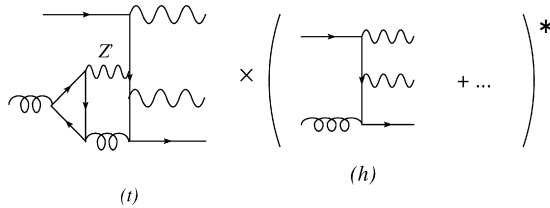


Fig. 16. Another configuration for the total amplitude of the $qg \rightarrow \gamma\gamma q$ process.

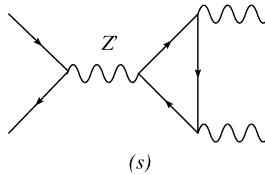


Fig. 17. Single diagram with an exchanged Z' boson in the s -channel.

between Fig. 19(a) and (b), does not erase the growth of the BIM amplitude, as discussed by us in a previous work. This mismatch is at the origin of the unitarity bound for this theory [13]. The identification of this scale in the context of QCD is quite subtle, since the lack of unitarity in a partonic process implies a violation of unitarity also at hadron level, but at a different scale compared to the partonic one, which needs to be determined numerically directly from the total hadronic cross section σ_{pp} . Overall, the convolution of a BIM amplitude with the parton distributions will cause a suppression of the rising partonic contributions, due to the small gluon density at large Bjorken x . Therefore, the graphs do not generate a large anomalous signal in this channel. However, the problem of unitarizing the theory by the inclusion of higher dimensional operators beyond the minimal dimension-5 operator $bF \wedge F$ remains.

The anomalous terms, beside the (n)(n)* contribution with the exchange of an extra Z/Z' which carry an anomalous component, which is $O(\alpha_{em}^2 \alpha_s \alpha_w^2)$, include the interference between

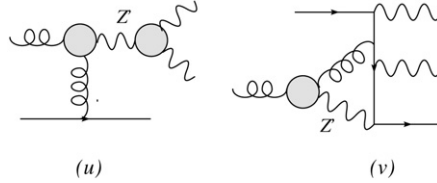


Fig. 18. Generic representation of the $qg \rightarrow \gamma\gamma$ process in the presence of a GS vertex of the AVV type.

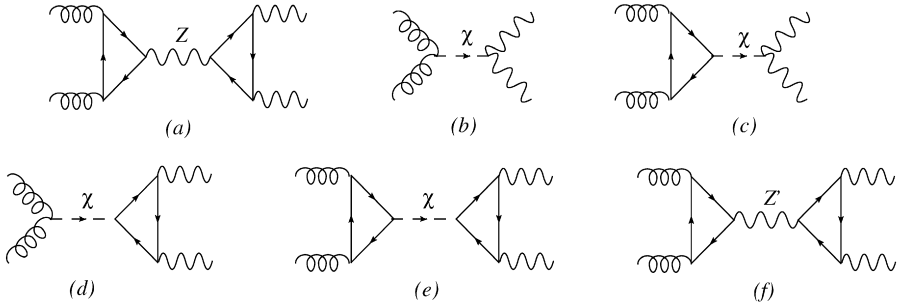


Fig. 19. Complete list of amplitudes included in the type of graphs shown in Fig. 14. They also have the exchange of a physical axion and contributions proportional to the mass of the internal fermion.

the $s/t/u$ box diagrams of $gg \rightarrow \gamma\gamma$ with the same BIM amplitude (n). In the gg sector the anomalous terms give, generically, an expression of the form

$$\sigma_{gg}^{an} = \alpha_{em}^2 (a_1 \alpha_s^2 \alpha_w + a_2 \alpha_s^2 \alpha_w^2), \tag{32}$$

with the first contribution coming from (n)(o)* and from the interference with the $(gg \rightarrow \gamma\gamma)$ box diagram, while the second from (n)(n)*. Other contributions which appears at $O(\alpha_{em}^2 \alpha_s^3 \alpha_w^2)$ (in the amplitude squared), are those shown in Fig. 15 which involve 2 anomaly diagrams (r) and their interference with the NLO real emission diagram of type (m). These contributions are phase-space suppressed. If we impose isolation cuts on the amplitude we can limit our analysis, for the anomalous signal, only to 2-to-2 processes near the photon.

4.1. Numerical analysis for direct photons

In our numerical implementation of double prompt photon production we compare the size of the anomalous corrections respect to the SM background evaluated by a Monte Carlo [15, 16]. Since the anomalous signal is small compared to that of the SM, we have extracted both for the SM case and the anomalous case the gg sector and compared them at hadron level by convoluting the partonic contributions with the PDF's. In this comparison, the SM sector is given by the graphs shown in Fig. 13 plus the interference graphs shown in Fig. 14. In the SM case this second set of graphs contributes proportionally to the mass of the heavy quarks in the anomaly loop. At high energy the hard scatterings coming from this interference are essentially due to the mass of the top quark running inside a BIM amplitude and are, therefore, related to heavy quark effects. In the anomalous case the same set of graphs is considered, but now the anomaly contributions are explicitly included. The hadronic differential cross section due to the anomalous

interactions for massless quarks is given by

$$\begin{aligned} \frac{d\sigma}{dQ} &= \int_0^{2\pi} d\phi \int_{-1}^1 d\cos\theta \frac{\tau}{4Q} \int_{\tau}^1 \frac{dx}{x} \Phi_{gg}\left(\frac{\tau}{x}\right) \Delta(x, \theta), \\ \Phi_{gg}(y) &= \int_y^1 \frac{dz}{z} g(y/z)g(z), \\ \Delta(x) &= \delta(1-x) \left[\frac{d\sigma_Z}{d\cos\theta} + \frac{d\sigma_{Z'}}{d\cos\theta} + \frac{d\sigma_{\chi}}{d\cos\theta} + \frac{d\sigma_{\text{int}}}{d\cos\theta} \right], \\ \frac{d\sigma_{\text{int}}}{d\cos\theta} &= \frac{d\sigma^{Z,\text{box}}}{d\cos\theta} + \frac{d\sigma^{Z',\text{box}}}{d\cos\theta} + \frac{d\sigma^{\chi,\text{box}}}{d\cos\theta}. \end{aligned} \tag{33}$$

The contributions which are part of this sector due to exchange of a Z or a Z' and a χ (see (a), (b) and (f) of the BIM set in Fig. 19) are those labelled above, while σ_{int} refers to the interferences shown in Fig. 14, with the inclusion of a Z' and a physical axion (such as Fig. 19(b)).

Defining

$$\sigma_{gg \rightarrow \gamma\gamma} \equiv \int_0^{2\pi} d\phi \int_{-1}^1 d\cos\theta \Delta(x, \theta) \tag{34}$$

the hadronic cross section takes the form of a product of the gluon luminosity and the partonic $gg \rightarrow \gamma\gamma$ cross section

$$\frac{d\sigma}{dQ} = \frac{Q}{4S} \sigma_{gg \rightarrow \gamma\gamma} \Phi(\tau). \tag{35}$$

4.2. The gg sector

Coming to the analysis of the gluon fusion sector, the result of this study is shown in Fig. 20 where we plot the gluon contribution to the hadronic cross section for both the SM and the MLSOM, having chosen $M_1 = 1$ TeV. We have used the MRST99 set of parton distributions to generate the NNLO gluon luminosity with $\alpha_s(M_Z) = 0.1175$, $Q = \frac{1}{2}\mu_R$ and $\sqrt{S} = 14$ TeV. We have chosen $\tan\beta = 40$ and different values of g_B . The size of the cross section is around 10^{-6} [pb/GeV] – right on the mass of the resonance – for both models, with a difference that grows as we rise the coupling constant for the anomalous $U(1)$ (g_B). We have chosen four possible values for g_B : a small parametric value ($g_B = 0.1$); equal to the coupling of the hypercharge g_Y at the same scale ($g_B = g_Y$) or to the $SU(2)_w$ coupling g_2 ($g_B = g_2$) or, finally, parametrically sizeable, with $g_B = 1$. In the interference graphs used for this comparison between the anomalous signal of the MLSOM and the SM (in this second case the BIM amplitudes contribute via the heavy quark mass in the loops) we have included, beside the BIM amplitude, the entire set of contributions shown in Fig. 19, with the exchange of a Z , a Z' and the axi-Higgs χ . We have chosen a light Stückelberg axion with $m_{\chi} = 30$ GeV. We show a more detailed investigation of the results for the various contributions in the gg sector in Fig. 21(a), (b). The dotted lines are the results obtained by the Monte Carlo and include both 2-to-2 and 2-to-3 contributions (pure QCD) with and without cuts, computed at LO and at NLO. The size of these contributions is around 2×10^{-6} pb/GeV in the SM case. We show in the same subfigure the anomalous corrections in

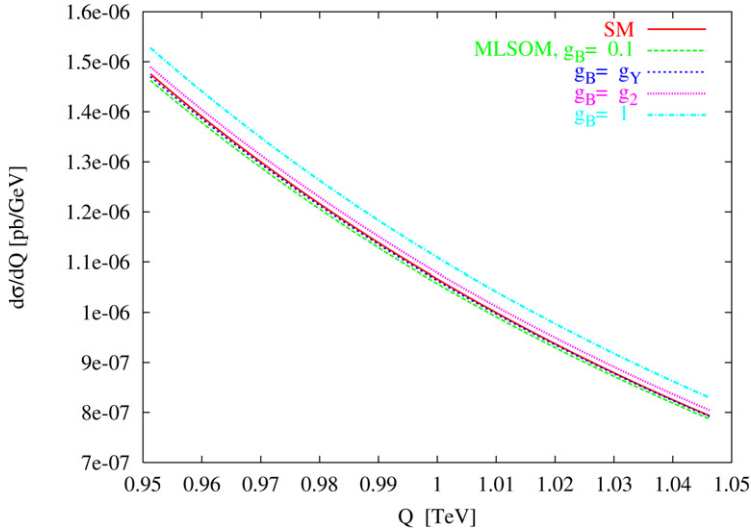


Fig. 20. Comparison plots for the gluon sector in the SM and in the anomalous model for a resonance of 1 TeV. The box-like contributions are not included, while they appear in the interference with the BIM amplitudes.

the MLSOM, which vary between 10^{-9} and 10^{-7} pb/GeV. Therefore, for $g_B \sim 1$, the anomalous sector of the MLSOM (the square of the box terms here are not included for the MSLOM) is suppressed by a factor of 10 respect to the signal from the same sector coming from the SM. In (b) we show the same contributions but we include in the SM also the quark channel (shown separately from the gluon channel), which is around 10^{-4} pb/GeV. Therefore, the quark sector overshadows the anomalous corrections by a factor of approximately 10^3 , which are difficult to extract at this value of the invariant mass.

5. Summary and conclusions

Both DY and DP have some special features, being characterized by a clean final state. In DY the identification of a new resonance in the neutral current sector would bring to the immediate conclusion that an extra Z' is present in the spectrum, but would give not specific indication concerning its true nature. Current experimental bounds constrain the mixing of a possible extra neutral component with the Z gauge boson, with a mass which should be larger than 900 GeV, rendering the future search of extra neutral interactions, at least for DY, quite delicate, being the allowed mass range at the tail of the invariant mass distribution of this process. This limit can be much lower in a certain class of models (see Ref. [11]).

Under these conditions, deciding over the true nature of the extra Z' , whether anomalous or not, would then be far more challenging and would require a parallel study of several independent channels. For this reason we have analyzed two processes which are both affected by anomalous contributions and could be used for correlated studies of the same interaction.

We have seen that changes in the factorization/renormalization scales both in the hard scatterings and in the evolution of the PDF's can easily overshadow the anomalous corrections, making a NLO/NNLO analysis truly necessary. We have concentrated our investigation on an extra Z' of 1 TeV in mass and searched for anomalous effects in the invariant mass distributions on the Z peak, at 1 TeV and for large Q values (up to 2 TeV's). We have shown that precision studies

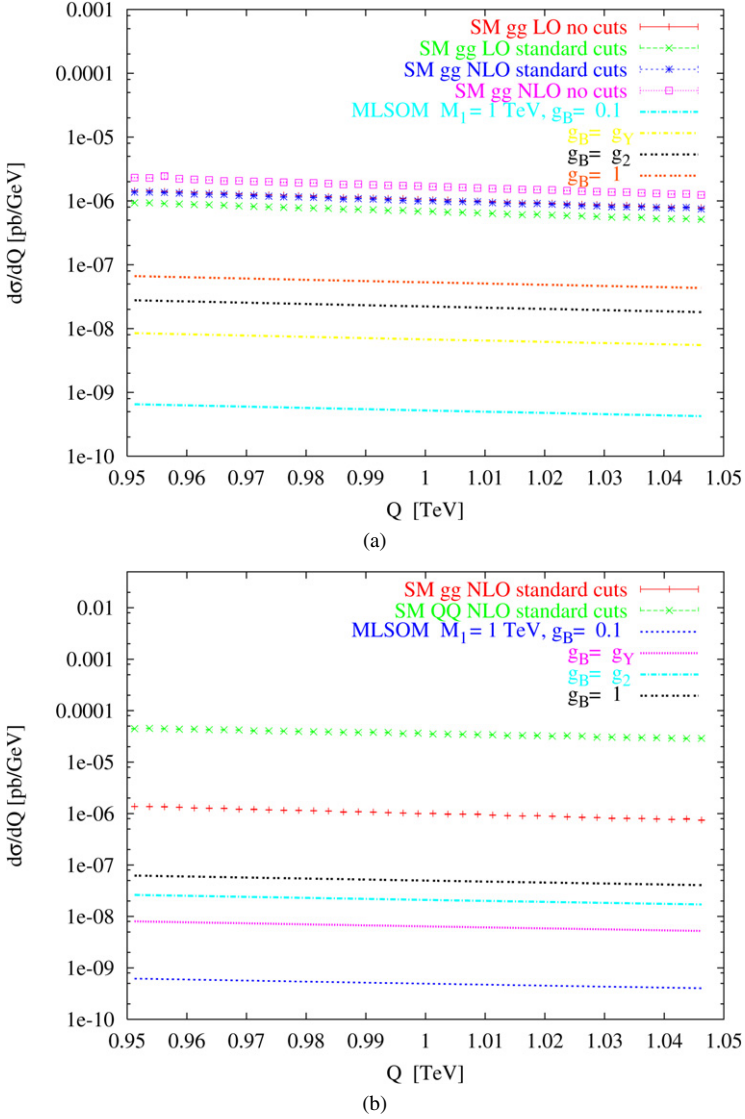


Fig. 21. (a): SM contributions for the gluon–gluon channel obtained with the Monte Carlo GAMMA2MC. These are indicated by dotted lines and include all the interferences and the box graphs. Shown are also the anomalous contributions of the MLSOM (no box). (b): as in (a) but we have included the Monte Carlo results for the SM qq channel at NLO.

on the Z resonance can be used to exclude some of the extra Z prime models due to the specific charge assignments, for a sizeable value of the coupling constant. We have presented results in which it is evident that the overlap region between the SM and the new extra Z prime model analyzed in this study tends to shrink when the anomalous coupling increases ($g_B \approx 1$). It is then clear that it will be possible at the LHC, using these types of studies, to exclude a class of these models characterized by variations of the cross section of the Z resonance around the level of 4%. This is an indetermination allowed both by the NNLO QCD K -factors and by the dependence of the result on the factorization and renormalization scales. The study that we have performed

can be easily specialized to the case of a typical linear collider, where, instead, anomaly effects, using our approach, are likely to be seen or discarded. More details on our analysis can be found in the ArXive version of this work [42].

Acknowledgements

We thank Nikos Irges for discussions. We thank Carl Schmidt for help on the use of the GAMMA2MC code for the NNLO study of the QCD background in di-photon and J.P. Guillet for exchanges concerning DIPHOX. The work of C.C. was supported in part by the European Union through the Marie Curie Research and Training Network “Universenet” (MRTN-CT-2006-035863) and by The Interreg II Crete-Cyprus Program.

References

- [1] P. Langacker, arXiv: 0801.1345.
- [2] C. Corianò, N. Irges, E. Kiritsis, Nucl. Phys. B 746 (2006) 77, hep-ph/0510332.
- [3] C. Corianò, N. Irges, Phys. Lett. B 651 (2007) 298, hep-ph/0612140.
- [4] C. Corianò, N. Irges, S. Morelli, JHEP 0707 (2007) 008, hep-ph/0701010.
- [5] C. Corianò, N. Irges, S. Morelli, Nucl. Phys. B 789 (2008) 133, hep-ph/0703127.
- [6] P. Anastopoulos, F. Fucito, A. Lionetto, G. Pradisi, A. Racioppi, Y.S. Stanev, arXiv: 0804.1156.
- [7] J. De Rydt, J. Rosseel, T.T. Schmidt, A. Van Proeyen, M. Zagermann, Class. Quantum Grav. 24 (2007) 5201, arXiv: 0705.4216.
- [8] J. De Rydt, T.T. Schmidt, M. Trigiante, A. Van Proeyen, M. Zagermann, arXiv: 0808.2130.
- [9] D. Feldman, Z. Liu, P. Nath, JHEP 0611 (2006) 007, hep-ph/0606294.
- [10] D. Feldman, Z. Liu, P. Nath, Phys. Rev. Lett. 97 (2006) 021801, hep-ph/0603039.
- [11] D. Feldman, Z. Liu, P. Nath, Phys. Rev. D 75 (2007) 115001, hep-ph/0702123.
- [12] J. Kumar, A. Rajaraman, J.D. Wells, Phys. Rev. D 77 (2008) 066011, arXiv: 0707.3488.
- [13] C. Corianò, M. Guzzi, S. Morelli, Eur. Phys. J. C 55 (2008) 629, arXiv: 0801.2949 [hep-ph].
- [14] A. Cafarella, C. Corianò, M. Guzzi, Comput. Phys. Commun. 179 (2008) 665, arXiv: 0803.0462 [hep-ph].
- [15] T. Binoth, J.P. Guillet, E. Pilon, M. Werlen, Eur. Phys. J. C 16 (2000) 311, hep-ph/9911340.
- [16] Z. Bern, L.J. Dixon, C. Schmidt, Phys. Rev. D 66 (2002) 074018, hep-ph/0206194.
- [17] C. Corianò, L.E. Gordon, Nucl. Phys. B 469 (1996) 202, hep-ph/9601350.
- [18] B. Kors, P. Nath, Phys. Lett. B 586 (2004) 366, hep-ph/0402047.
- [19] D.M. Ghilencea, L.E. Ibanez, N. Irges, F. Quevedo, JHEP 0208 (2002) 016, hep-ph/0205083.
- [20] L.E. Ibanez, F. Marchesano, R. Rabadan, JHEP 0111 (2001) 002, hep-th/0105155.
- [21] R. Armillis, C. Corianò, M. Guzzi, S. Morelli, JHEP 0810 (2008) 034, arXiv: 0808.1882 [hep-ph].
- [22] T.J. Allen, M.J. Bowick, A. Lahiri, Mod. Phys. Lett. A 6 (1991) 559.
- [23] R. Armillis, C. Corianò, M. Guzzi, JHEP 0805 (2008) 015, arXiv: 0711.3424 [hep-ph].
- [24] N.N. Achasov, Phys. Lett. B 287 (1992) 213.
- [25] A.D. Dolgov, V.I. Zakharov, Nucl. Phys. B 27 (1971) 525.
- [26] M. Knecht, S. Peris, M. Perrottet, E. de Rafael, JHEP 0403 (2004) 035, hep-ph/0311100.
- [27] F. Jegerlehner, O.V. Tarasov, Phys. Lett. B 639 (2006) 299, hep-ph/0510308.
- [28] M. Knecht, S. Peris, M. Perrottet, E. de Rafael, JHEP 0211 (2002) 003, hep-ph/0205102.
- [29] R. Hamberg, W.L. van Neerven, T. Matsuura, Nucl. Phys. B 359 (1991) 343.
- [30] A. Cafarella, C. Corianò, M. Guzzi, JHEP 0708 (2007) 030, hep-ph/0702244.
- [31] A. Cafarella, C. Corianò, M. Guzzi, Nucl. Phys. B 748 (2006) 253, hep-ph/0512358.
- [32] W. Bernreuther, R. Bonciani, T. Gehrmann, R. Heinesch, T. Leineweber, E. Remiddi, Nucl. Phys. B 723 (2005) 91, hep-ph/0504190.
- [33] S.A. Larin, Phys. Lett. B 303 (1993) 113, hep-ph/9302240.
- [34] R.J. Gonçalves, C.M. Hung, J. Pawłowski, Phys. Rev. D 46 (1992) 4930.
- [35] P.J. Rijken, W.L. van Neerven, Phys. Rev. D 52 (1995) 149, hep-ph/9501373.
- [36] A.D. Martin, R.G. Roberts, W.J. Stirling, R.S. Thorne, Eur. Phys. J. C 23 (2002) 73, hep-ph/0110215.
- [37] A.D. Martin, R.G. Roberts, W.J. Stirling, R.S. Thorne, Phys. Lett. B 531 (2002) 216, hep-ph/0201127.

- [38] C. Corianò, A.E. Faraggi, M. Guzzi, *Phys. Rev. D* 78 (2008) 015012, arXiv: 0802.1792 [hep-ph].
- [39] M.S. Carena, A. Daleo, B.A. Dobrescu, T.M.P. Tait, *Phys. Rev. D* 70 (2004) 093009, hep-ph/0408098.
- [40] A. Cafarella, C. Corianò, M. Guzzi, *AIP Conf. Proc.* 964 (2007) 206, arXiv: 0709.2115.
- [41] T. Binoth, J.P. Guillet, E. Pilon, M. Werlen, hep-ph/0111043.
- [42] R. Armillis, C. Corianò, M. Guzzi, S. Morelli, arXiv: 0811.0117 [hep-ph].